A Closer View of the Radio-FIR Correlation: Disentangling the Contributions of Star Formation and Active Galactic Nucleus Activity

Morić, I.; Smolčić, Vernesa; Kimball, A.; Riechers, D. A.; Ivezić, Ž.; Scoville, N.

A CLOSER VIEW OF THE RADIO–FIR CORRELATION: DISENTANGLING THE CONTRIBUTIONS OF STAR FORMATION AND ACTIVE GALACTIC NUCLEUS ACTIVITY[*]

I. MORIĆ[1,2], V. SMOLČIĆ[2,3,4,7], A. KIMBALL[5,6], D. A. RIECHERS[2,8], Ž IVEZIĆ[5], AND N. SCOVILLE[2]
[1] Physics Department, University of Zagreb, Bijenička cesta 32, 10002 Zagreb, Croatia
[2] California Institute of Technology, MC 249-17, 1200 East California Boulevard, Pasadena, CA 91125, USA
[3] European Southern Observatory, Karl-Schwarzschild-Strasse 2, 85748 Garching b. Muenchen, Germany
[4] Argelander Institut for Astronomy, Auf dem Hügel 71, Bonn, 53121, Germany
[5] Department of Astronomy, University of Washington, Box 351580, Seattle, WA 98195-1580, USA
[6] National Radio Astronomy Observatory, 520 Edgemont Road, Charlottesville, VA 22903, USA

ABSTRACT

We extend the Unified Radio Catalog, a catalog of sources detected by various (NVSS, FIRST, WENSS, GB6) radio surveys, and SDSS, to IR wavelengths by matching it to the *IRAS* Point and Faint Source catalogs. By fitting each NVSS-selected galaxy's NUV-NIR spectral energy distribution (SED) with stellar population synthesis models we add to the catalog star formation rates (SFRs), stellar masses, and attenuations. We further add information about optical emission-line properties for NVSS-selected galaxies with available SDSS spectroscopy. Using an NVSS 20 cm ($F_{1.4\,GHz} \gtrsim 2.5$ mJy) selected sample, matched to the SDSS spectroscopic ("main" galaxy and quasar) catalogs and *IRAS* data ($0.04 < z \lesssim 0.2$) we perform an in-depth analysis of the radio–FIR correlation for various types of galaxies, separated into (1) quasars, (2) star-forming, (3) composite, (4) Seyfert, (5) LINER, and (6) absorption line galaxies using the standard optical spectroscopic diagnostic tools. We utilize SED-based SFRs to independently quantify the source of radio and FIR emission in our galaxies. Our results show that Seyfert galaxies have FIR/radio ratios lower than, but still within the scatter of, the canonical value due to an additional (likely active galactic nucleus (AGN)) contribution to their radio continuum emission. Furthermore, IR-detected absorption and LINER galaxies are on average strongly dominated by AGN activity in both their FIR and radio emission; however their average FIR/radio ratio is consistent with that expected for star-forming galaxies. In summary, we find that most AGN-containing galaxies in our NVSS–*IRAS*–SDSS sample have FIR/radio flux ratios indistinguishable from those of the star-forming galaxies that define the radio–FIR correlation. Thus, attempts to separate AGNs from star-forming galaxies by their FIR/radio flux ratios alone can separate only a small fraction of the AGNs, such as the radio-loud quasars.

Key words: cosmology: observations – evolution – galaxies: active – galaxies: fundamental parameters – radio continuum: galaxies

Online-only material: color figures

1. INTRODUCTION

The radio–FIR correlation is one of the tightest correlations in observational astrophysics (e.g., Helou et al. 1985; Condon 1992; Mauch & Sadler 2007; Yun et al. 2001; Bell 2003; Sargent et al. 2010; Kovacs et al. 2006; Murphy et al. 2009; Appleton et al. 2004). The correspondence between the radiation in the (far-)infrared and that in the radio spans over nearly five orders of magnitude in various types of galaxies, ranging from dwarfs to ULIRGs. Given that the two observational windows, IR and radio, trace independent and different intrinsic physical mechanisms in galaxies—thermal versus synchrotron radiation—the existence of such a tight correspondence is remarkable. It is generally believed that recent star formation in galaxies is the process that relates IR and radio emission.

The radio–FIR correlation has been extensively studied in the past both in the low- (Helou et al. 1985; Condon 1992; Garrett 2002; Mauch & Sadler 2007; Yun et al. 2001; Bell 2003) and high-redshift universe (Sargent et al. 2010; Michałowski et al. 2010; Kovacs et al. 2006; Sajina et al. 2008; Murphy et al. 2009; Appleton et al. 2004; Vlahakis et al. 2008; Ibar et al.

2008; Chapman et al. 2005). It has been shown that, out to redshifts of $z \sim 3$–4, the FIR/radio ratios of various types of galaxies are essentially the same as those in the local universe. At higher redshifts, radio-quiet QSOs have been demonstrated to have FIR/radio ratios consistent with the local value, while the FIR/radio ratios of $z > 4$ SMGs are found to be lower by a few factors. This is somewhat contrary to expectations, as the FIR/radio ratio is expected to be rising with redshift (especially at $z \gtrsim 3$) due to the increase of the cosmic microwave background (CMB) energy density (U_{CMB}) with redshift, $U_{CMB} \propto (1 + z)^4$, which suppresses the non-thermal component of a galaxy's radio continuum via inverse-Compton (IC) scattering (see Murphy 2009 for details). An explanation for this discrepancy can be provided by additional processes that add to a galaxy's radio continuum, such as increased magnetic field strengths or AGN contribution, that may compensate for the radio continuum emission losses due to IC scattering.

The AGN contribution to the radio–FIR correlation has been studied in the past to some extent. Typically a low FIR/radio ratio, significantly offsetting a galaxy from the correlation, is thought to indicate a radio-loud AGN (e.g., Yun et al. 2001; Condon et al. 2002). However, recent studies have shown that optically selected AGNs often follow the correlation, albeit with a slightly lower FIR/radio ratio. For example, based on SDSS–NVSS–*IRAS* data, Obrić et al. (2006) have demonstrated a tight correlation between radio and 60 μm fluxes for low-

luminosity AGNs (predominantly Seyferts and LINERs), which varies by only ∼20% relative to that of star-forming galaxies. Utilizing 6dFGS-NVSS-*IRAS* data, Mauch & Sadler (2007) inferred a lower average FIR/radio ratio for AGN-bearing galaxies (Seyferts, LINERS, and quasars), but still within the scatter of the correlation for star-forming galaxies. Furthermore, studies of the correlation at higher redshifts have yielded a handful of interesting objects for which it has clearly been shown that a significant AGN contribution to IR and/or radio exists, yet their FIR/radio ratio is consistent with the canonical value for star-forming galaxies (Riechers et al. 2009; Murphy et al. 2009).

In order to understand in more detail the contribution of AGN activity to the radio–FIR correlation, we perform an in-depth study of the radio–FIR correlation, with a large sample, as a function of galaxy type, and comparison with star formation rates (SFRs) for those individual samples. The various types of star-forming and AGN-bearing galaxies have been drawn from the NVSS (Condon et al. 1998), *IRAS* (Neugebauer et al. 1984), and Sloan Digital Sky Survey (SDSS; York et al. 2000) sky surveys. In Section 2, we present the data used in this paper. We present the correlation for various types of galaxies in Section 3. In Section 4, we link the FIR and radio emission from galaxies in our sample to independently derived SFRs, and in Section 5 and Section 6 we discuss and summarize our results, respectively. We adopt $H_0 = 70$, $\Omega_M = 0.3$, $\Omega_\Lambda = 0.7$, and define the radio synchrotron spectrum as $F_\nu \propto \nu^{-\alpha}$, assuming $\alpha = 0.7$. Throughout the text we will often use the term "quasar" referring to both quasi-stellar radio sources and quasi-stellar objects.

2. DATA AND GALAXY SAMPLES: EXPANDING THE UNIFIED RADIO CATALOG

2.1. Unified Radio Catalog

Kimball & Ivezić (2008) have constructed a catalog of radio sources detected by the GB6 (6 cm), FIRST (Becker et al. 1995), NVSS (Condon et al. 1998; 20 cm), and WENSS (92 cm) radio surveys, as well as the SDSS (DR6) optical survey (York et al. 2000). This "Unified Radio Catalog" has been generated in such a way that it allows a broad range of 20 cm based sample selections and source analysis (see Kimball & Ivezić 2008 for details). The 2.7 million entries are comprised of the closest three FIRST to NVSS matches (within 30″) and vice versa, as well as unmatched sources from each survey. All entries have been supplemented by data from the other radio and optical surveys, where available. Here we select from the Unified Radio Catalog (version 1.1) all 20 cm sources that have been detected by the NVSS radio survey (using matchflag_nvss = −1 and matchflag_first ⩽ 1; see Kimball & Ivezić 2008 for details). This selection yields a radio flux limited ($F_{1.4\,\mathrm{GHz}} \gtrsim 2.5$ mJy) sample that contains 1,814,748 galaxies. In the following section, we expand this catalog to IR wavelengths, and augment it with additional (spectroscopic and SED-based) information.

2.2. Expanding the Unified Radio Catalog

2.2.1. IRAS

For the purpose of this paper, we have expanded the Unified Radio Catalog to IR wavelengths by cross-correlating it with the *IRAS* point-source and faint-source catalogs (hereafter PSC and FSC, respectively). The *IRAS* PSC contains 245,889 confirmed point sources detected at 12, 25, 60 and 100 μm, respectively (Strauss et al. 1990). The completeness of the catalog at
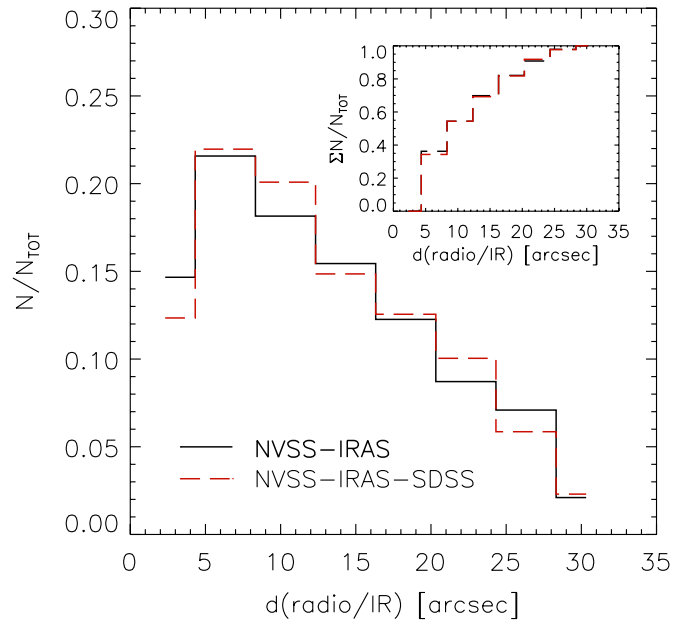

Figure 1. Distribution of distances between the radio and FIR detections for the NVSS-*IRAS* (full black line) and NVSS–SDSS–*IRAS* (dashed red line) samples. The cumulative distribution is shown in the inset.

(A color version of this figure is available in the online journal.)

these wavelengths reaches down to 0.4, 0.5, 0.6, and 1.0 Jy, respectively. The FSC was tuned to fainter levels based on the same IR data by point-source filtering the individual detector data streams and then co-adding those using a trimmed-average algorithm (see Moshir et al. 1992). The reliability of the FSC is slightly lower than that of the PSC ($\gtrsim$ 94% compared to 99.997%); however its sensitivity is higher by a factor of ∼2.5. The FSC contains 173,044 point sources with flux densities typically greater than 0.2 Jy at 12, 25, and 60 μm and 0.5 Jy at 100 μm.

We used matching radius of 30″, as optimized by Obrić et al. (2006), in cross-correlating the Unified Radio Catalog with the IR *IRAS* data. In Figure 1, we show the distribution of the distances between the IR and radio detections. The cumulative distribution displayed in Figure 1 shows that ∼70% of the positional matches are within an angular distance of 15″.

Our NVSS-selected radio sample contains 18,313 galaxies with high quality IR photometry[9] (see Table 1). As the FSC and PSC have been generated based on the same data, most of the PSC sources are included in the FSC. In our entire NVSS-*IRAS* sample, 26% of the sources have a PSC detection but are not included in the FSC. This fraction, however, reduces to only 3% after an optical (SDSS) cross-match is performed.

The 60 and 100 μm magnitudes reported in the PSC and FSC are in agreement for the union of the two IR samples. The biweighted mean of the flux difference (for a subsample with SDSS detections) is 0.02 and 0.03 Jy at 60 and 100 μm, respectively. The root mean scatter of the 60 μm flux difference distribution is 0.06 Jy, while that of the 100 μm distribution is significantly larger, i.e., 0.16 Jy. Therefore, in order to access the highest quality IR photometry, hereafter we use the values reported in either the FSC or PSC catalog corresponding to the higher photometric quality flag quoted in the catalogs. The

---

[7] We take the *IRAS* quality indicator, reported in the FSC and PSC, to be ⩾2 at 60 and 100 μm (the wavelength bands utilized here).

Table 1
Sample Summary

	IRAS (FSC + PSC)	SDSS (MAIN + QUASAR)	*IRAS*–SDSS
Total radio sample	18313	9591	524
Quasars	⋯	4490	21
Absorption	⋯	3072	16
Composite	⋯	654	203
SF unambiguous	⋯	621	216
SF ambiguous	⋯	9	0
AGN unambiguous	⋯	454	43
AGN ambiguous	⋯	291	25
Seyfert unambiguous	⋯	200	37
LINER unambiguous	⋯	254	6

Notes. The first column denotes the number of radio—*IRAS* (Point Source, PS, and Faint Source, FS) catalog with high quality IR photometry. The second column shows the number of sources in the radio—SDSS ("main" and quasar) catalog, and the third column is the matched radio–SDSS ("main" and quasar)–*IRAS* catalog. The rows indicate the various galaxy types we separate the objects into. The unambiguous/ambiguous selection is based on various spectroscopic diagnostic tools (see Figure 5 and the text for details). The shown numbers are limited to the $0.04 < z < 0.3$ redshift range.
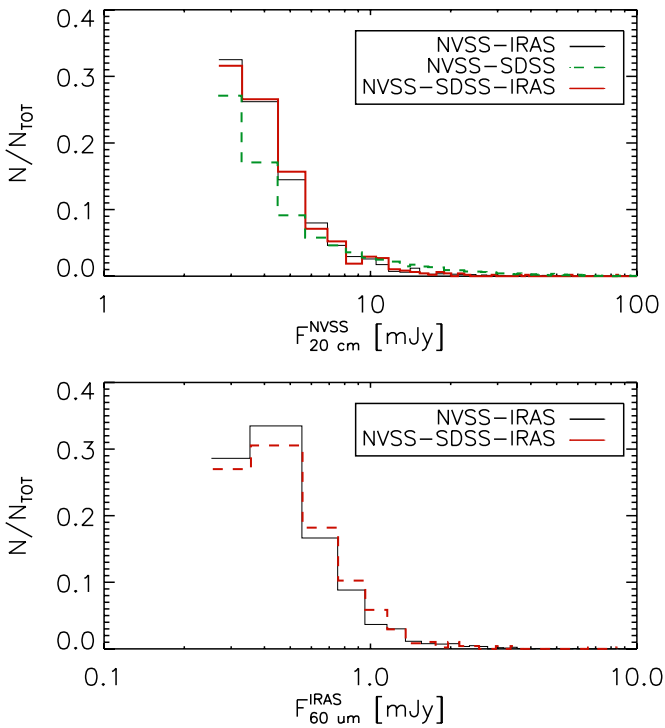

Figure 2. Distribution of flux density at 20 cm (top panel) and 60 μm (bottom panel) for various radio-selected samples indicated in the top right of the panels. (A color version of this figure is available in the online journal.)

Figure 3. Top panel shows the 1.4 GHz luminosity as a function of redshift for the NVSS–SDSS galaxies. The bottom panel shows their absolute optical *r*-band magnitude (not *K*-corrected) as a function of redshift.

distribution of the 60 μm and 20 cm flux densities is shown in Figure 2.

2.2.2. SDSS Quasar and Main Galaxy Sample Catalogs

We have further matched the NVSS-selected sample from the Unified Radio Catalog with data drawn from (1) the SDSS DR5 quasar sample (Schneider et al. 2007), and (2) the DR4 "main" spectroscopic sample for which derivations of emission-line fluxes from the SDSS spectra are available (see Smolčić et al. 2009 and references therein; note that the DR5 quasar and DR4 main galaxy catalogs were the most up-to-date versions available at the time). The latter was complemented with stellar
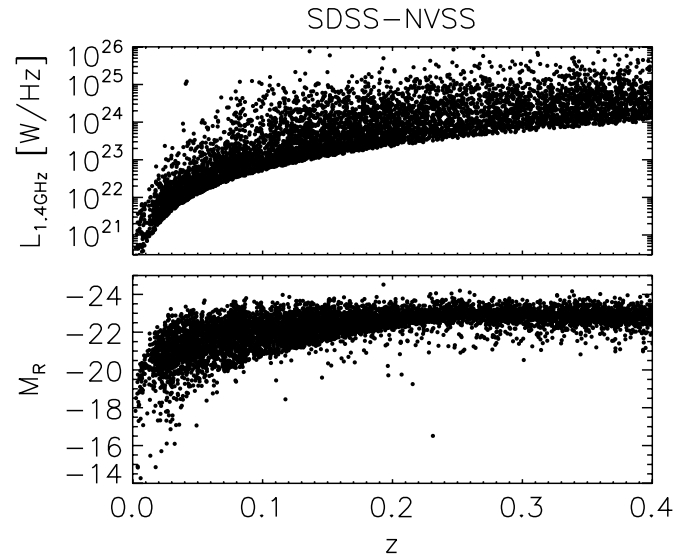
masses, SFRs, dust attenuations, ages, metallicities, and a variety of other parameters based on spectral energy distribution (SED) fitting of the SDSS (*ugriz*) photometry using the Bruzual et al. (2003) stellar population synthesis models. The SED fitting was performed as described in detail in Smolčić et al. (2008).

During the inspection of the validity of the final catalog, we have found about 1% of objects with different spectroscopic redshifts in various SDSS data releases ($\Delta z > 5 \times 10^{-4}$). We have excluded those from the sample. Furthermore, a small number (∼0.2%) of duplicate objects was present in both the SDSS "main" galaxy sample and the SDSS Quasar Catalog. Visually inspecting their spectra yielded that most of these objects are better matched to the properties of the "main" galaxy sample (as no power-law continuum nor broad emission lines were present in the spectrum), and we have excluded these from our quasar sample. A summary of the various radio–IR–optical samples is given in Table 1, and in Figure 3 and Figure 4 we show the radio (20 cm), optical (*r* band), and far-IR luminosities as a function of redshift for the final NVSS–SDSS
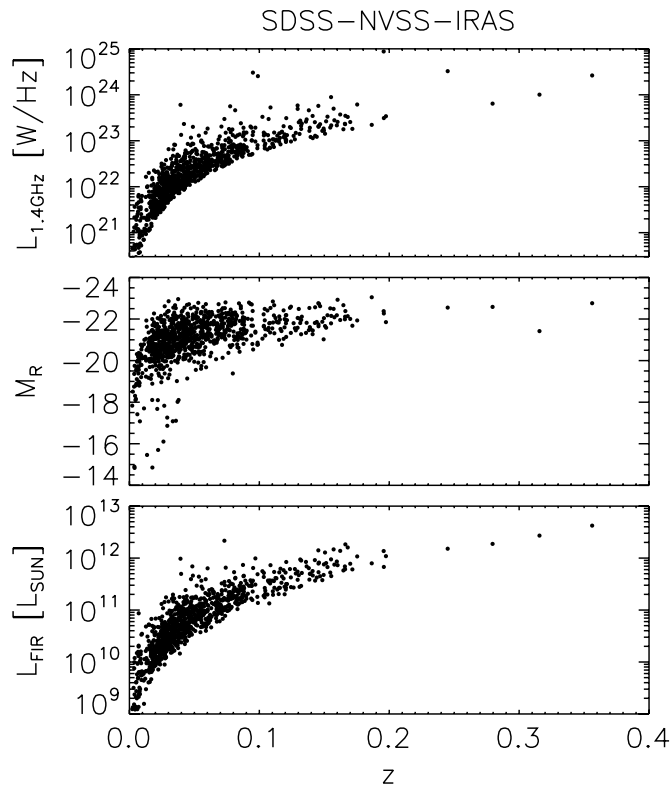
Figure 4. Top two panels are the same as Figure 3 but for NVSS–SDSS–*IRAS* galaxies. The bottom panel shows the FIR luminosity vs. redshift.

and NVSS–SDSS–*IRAS* samples (see Equations (3) and (4)). Note that the shallow *IRAS* sensitivity (compared to the NVSS and SDSS data) significantly reduces the number of objects, and biases the sample toward lower redshifts.

2.3. Radio–Optical–IR Samples

2.3.1. Star-forming and AGN Galaxy Subsamples

We have used the optical spectroscopic information added to the NVSS selected sample to spectroscopically separate the galaxies present in the SDSS (DR4) "main" galaxy sample as absorption line, AGN (LINER/Seyfert), star-forming, or composite galaxies.

We define emission-line galaxies as those where the relevant emission lines (Hα, Hβ, O[III,λ5007], N[II,λ6584], S[II,$\lambda\lambda$6717,6731]) have been detected at S/N $\geqslant$ 3, and consider all galaxies with S/N < 3 in any of these lines as absorption line systems (see e.g., Best et al. 2005; Kewley et al. 2006; Smolčić et al. 2009). As strong emission lines are not present in the spectra of the latter, yet they are luminous at 20 cm, they can be considered to be (low excitation) AGNs (see e.g., Best et al. 2005; Smolčić et al. 2008 for a more detailed discussion). Furthermore as illustrated in Figure 5, using standard optical spectroscopic diagnostics (Baldwin et al. 1981; Kauffmann et al. 2003; Kewley et al. 2001, 2006) we sort the emission-line galaxies into (1) star-forming, (2) composite, (3) Seyfert, and (4) LINER galaxies. The last two classes have been selected "unambiguously" by requiring combined criteria using three emission-line flux ratios (see the middle and right panels in Figure 5). A summary of the number of objects in each class is given in Table 1. It is noteworthy that the IR detection fraction is a strong function of spectral class. It is the lowest for absorp-

tion line (0.6%) and LINER (6.5%) galaxies, intermediate for Seyferts (22%) and the highest for composite (40%) and star-forming (46%) galaxies. These results suggest lower amounts of dust (and gas; Solomon & Vanden Bout 2005) in the former or alternatively dominantly very cold dust that peaks at longer wavelengths.

The redshift distribution of the various galaxy types with 20 cm NVSS and NVSS-*IRAS* detections is shown in the two top panels in Figure 6. Note that the redshift distribution of 20 cm detected absorption line galaxies is biased toward higher redshifts, compared to all other galaxy types (see the top panel in Figure 6). However, this is not the case when an *IRAS* IR detection is required, as illustrated in the middle panel in Figure 6. The IR detection fraction of the different galaxy classes is shown as a function of redshift in the bottom panel in Figure 6. Except for the overall trend that absorption and LINER galaxies are detected less efficiently in the IR, there is no substantial difference between the detection fractions as a function of redshift for different types of spectroscopically selected galaxies.

Hereafter, we apply redshift range limits of 0.04 < z < 0.3 to our sample. The lower redshift limit is adopted from Kewley et al. (2005). Kewley et al. explored effects of fixed-size aperture of the SDSS spectroscopic fibers on the spectral characteristics such as metallicity, SFR, and reddening. They concluded that a minimum aperture size covering ≈20% of spectral light was required to properly approximate global values. The SDSS fiber aperture of 3″ diameter collects such a fraction of light for galaxies of average size, type, and luminosity at z $\gtrsim$ 0.04. The upper redshift limit of z = 0.3 is equivalent to that of the SDSS "main" spectroscopic sample (note however that the majority of IR-detected galaxies are at z < 0.2, see Figure 4). It is worth noting that, because of lower spectral signal to noise for fixed-luminosity galaxies at greater distances, galaxies with weak emission lines, such as LINERs, can get confused with absorption line galaxies at z > 0.1 (Kewley et al. 2005). However, as LINER and absorption galaxies have similar physical properties (e.g., Smolčić et al. 2009), we simply combine these two types of galaxies, and treat them hereafter as a single class.

2.3.2. Quasar Subsample

Matching the SDSS DR5 quasar catalog to the Unified radio catalog resulted in 4490 matches (see Table 1). The redshift range of our radio luminous quasars is 0.09–5.12, with a median at z = 1.36. Requiring *IRAS* detections biases the sample toward low redshifts (0.12 $\leqslant$ z $\leqslant$ 1.15), with a median redshift of 0.18, and selects only ∼0.5% of the radio-detected quasars. The radio ($\gtrsim 10^{23}$ W Hz^{-1}) and FIR ($\gtrsim$2 × 10^{11} $L_{\odot}$) luminosities (see Equations (3) and (4)) of our quasars are systematically higher than those of the SDSS "main" spectroscopic sample galaxies in our radio–optical–IR sample.

3. QUANTIFYING THE RADIO–FIR CORRELATION FOR VARIOUS SOURCE TYPES

3.1. Parameterizing the Radio–FIR Correlation

The radio–FIR correlation is usually quantified by its slope via the q parameter (Helou et al. 1985), defined as the logarithmic ratio of the far-infrared flux to radio flux density:

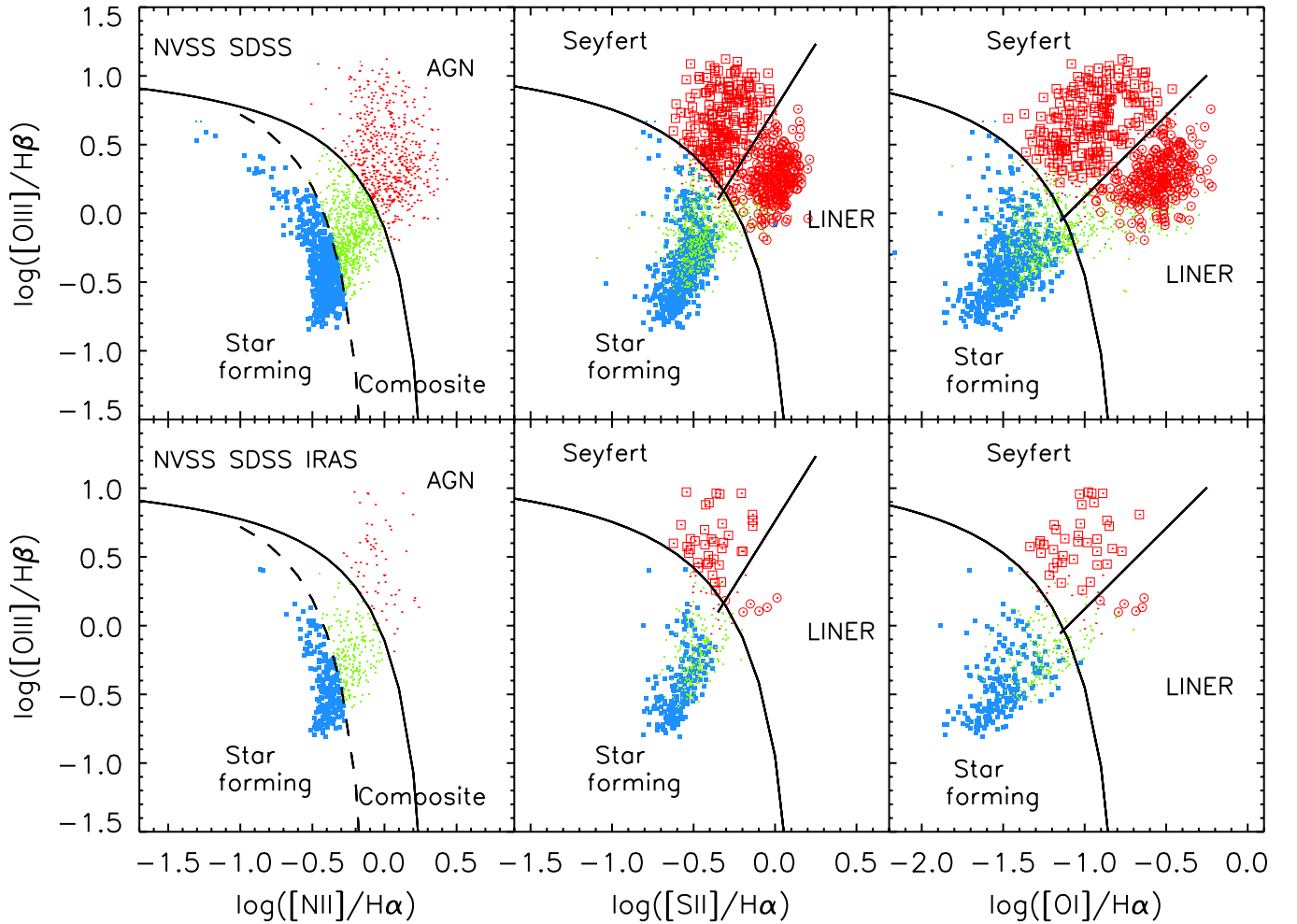$$q = \log \left\{ \frac{F_{\text{FIR}}/(3.75 \times 10^{12} \text{ Hz})}{F_{1.4 \text{ GHz}}} \right\}, \qquad (1)$$

Figure 5. Optical spectroscopic diagnostic diagrams (see Kauffmann et al. 2003; Kewley et al. 2001, 2006) that separate emission-line galaxies into star-forming, composite galaxies, and various types of AGNs (Seyferts and LINERs). The top panel shows the SDSS–NVSS sample, and the bottom panel the SDSS–NVSS–*IRAS* galaxies. Large symbols represent unambiguously identified galaxies (see the text for details). Blue filled squares represent SF galaxies and green dots show composites. Red open squares and circles represent unambiguous Seyferts and LINERs, respectively.

(A color version of this figure is available in the online journal.)

where $F_{1.4\,GHz}$ is the 1.4 GHz radio flux density in units of Wm^{-2}Hz^{-1} and F_{FIR} is the far-infrared flux in units of Wm^{-2}. Following Sanders & Mirabel (1996), we define the latter as

$$F_{FIR} = 1.26 \times 10^{-14}\,(2.58 S_{60\,\mu m} + S_{100\,\mu m}), \qquad (2)$$

where $S_{60\,\mu m}$ and $S_{100\,\mu m}$ are observed flux densities at 60 and 100 μm (in Jy), respectively.

We compute the far-infrared luminosity as

$$L_{FIR} = 4\pi D_L^2 C F_{FIR}\,[L_\odot], \qquad (3)$$

where D_L is the luminosity distance (in units of m) and C is a scale factor used to correct for the extrapolated flux longward of the *IRAS* 100 μm filter. We use $C = 1.6$ (see Table 1 in Sanders & Mirabel 1996). Note that this expression can also be utilized to compute the FIR luminosities for our IR-detected quasars, given their relatively low redshifts.

The radio luminosity density is computed as

$$L_{1.4\,GHz} = \frac{4\pi D_L^2}{(1+z)^{1-\alpha}} F_{1.4\,GHz}, \qquad (4)$$

where z is the redshift of the source, $F_{1.4\,GHz}$ is its integrated flux density, and α is the radio spectral index (assuming $F_\nu \propto \nu^{-\alpha}$).

To compute the radio luminosities, we assumed a spectral index of $\alpha = 0.7$.

3.2. Radio–FIR Correlation for All Sources

The radio–FIR correlation for the NVSS–SDSS–*IRAS* sample is summarized in Figure 7. The radio and FIR flux densities (top left panel) and luminosities (top right panel) clearly show a tight correlation that holds over many orders of magnitude. In the middle panels we show the q parameter, that characterizes the slope of the radio–FIR correlation (see Equation (1)), as a function of FIR and radio luminosities. The average q is constant as a function of FIR luminosity (middle left panel), and it is decreasing with increasing radio power (middle right panel; see also below). In the bottom panels of Figure 7, we show the q parameter as a function of redshift, as well as its distribution for all our NVSS–SDSS–*IRAS* sources (galaxies and quasars). We find that the average (biweighted mean) q-value for the entire NVSS–SDSS–*IRAS* sample is $q = 2.273 \pm 0.008$, with a root-mean-square scatter of $\sigma = 0.18$. This is in very good agreement with previous findings (Condon 1992; Yun et al. 2001; Condon et al. 2002; Bell 2003; Mauch & Sadler 2007), and will be discussed in more detail in Section 5.
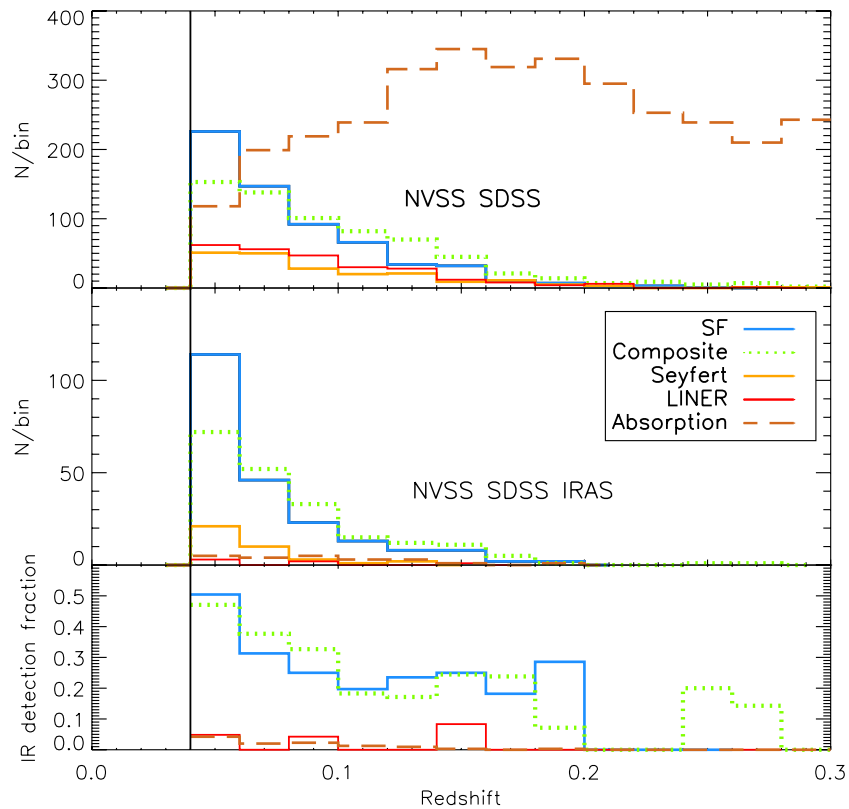
Figure 6. Redshift distribution of galaxies in the NVSS–SDSS (top panel) and NVSS–SDSS–*IRAS* (middle panel) samples. The bottom panel shows the IR detection fraction as a function of redshift. Various galaxy types are indicated in the top right of the middle panel.

(A color version of this figure is available in the online journal.)

The quasars in our sample comprise the high-luminosity end at both IR and radio wavelengths (they are also located at higher redshifts, compared to the IR- and radio-detected "main" galaxy sample). It is also obvious that there is a larger fraction of quasars that do not lie on the radio–IR correlation, compared to that for the "main" sample galaxies.

3.3. Radio–FIR Correlation for Different Types of Galaxies

In Figure 8, we present the radio–FIR correlation for the SDSS "main" galaxy sample subdivided into different, spectroscopically selected galaxy types (absorption, LINER, Seyfert, composite, and star-forming galaxies; see Section 2.3.1 and Figure 5 for details on the selection). The decrease in q with increasing radio power for all types of galaxies (middle right panel) is consistent with various other observations (e.g., Smolčić et al. 2008; Kartaltepe et al. 2010; Sargent et al. 2010; Ivison et al. 2010). Note that, given the definition of the FIR/radio ratio, for any sample in which q does not vary with FIR luminosity, and has a non-zero dispersion, it is expected to decrease with increasing radio luminosity (see, e.g., Condon 1984). To test whether the magnitude of the decrease is as expected from statistics or, e.g., higher due to an additional effect (such as AGN contribution) we have computed the radio luminosity for each source based on its observed FIR luminosity and an FIR/radio ratio drawn from a Gaussian distribution with a dispersion of 0.18 and a mean of 2.27. We find that the decrease of q with radio luminosity in the observed data is consistent with that in the simulated data, thus not requiring additional effects (such as increasing AGN contribution with increasing radio power) to explain this trend (at least in the radio luminosity range probed here).

A quantitative analysis of the radio–FIR correlation for different galaxy types is presented in Figure 9. The spectroscopic selection of pure star-forming galaxies allows us to quantify the radio–IR correlation in a rather unbiased manner. For our star-forming galaxies we find an average q value of $\langle q \rangle = 2.27 \pm 0.05$, with a small rms scatter of $\sigma = 0.13$. It is interesting to note that as the AGN contribution rises in galaxies (as inferred based on optical spectroscopic diagnostics) the scatter in q increases by $\sim$50% to $\sim$150%. Interestingly, the scatter is the highest for Seyfert types of galaxies, for which we also find the lowest average q-value, $\langle q \rangle = 2.14 \pm 0.05$. These differences will be further discussed in Section 5.

3.4. Radio–FIR Correlation for Quasars

In Figure 10, we quantify the radio–FIR correlation for the 21 IR-detected quasars in our sample. The distribution of the FIR/radio ratio cannot be well fit with a Gaussian distribution. The median q-value of the sample is 2.04, comparable to the average q value we have found for Seyfert galaxies (2.14), and lower than that for star-forming galaxies (2.27; see Figure 9). It is worth noting that the higher redshift quasars ($0.2 \lesssim z \lesssim 0.4$) appear to be biased toward more radio-loud AGNs.

4. AN INDEPENDENT VIEW OF THE RADIO–FIR CORRELATION: A LINK TO STAR FORMATION

It is generally taken that recent star formation drives both the radio and FIR emission of galaxies that lie on the radio–FIR correlation (Condon 1992; Mauch & Sadler 2007). Therefore, a correlation is expected to be present between the SFRs and radio/FIR luminosities obtained from the fluxes of galaxies
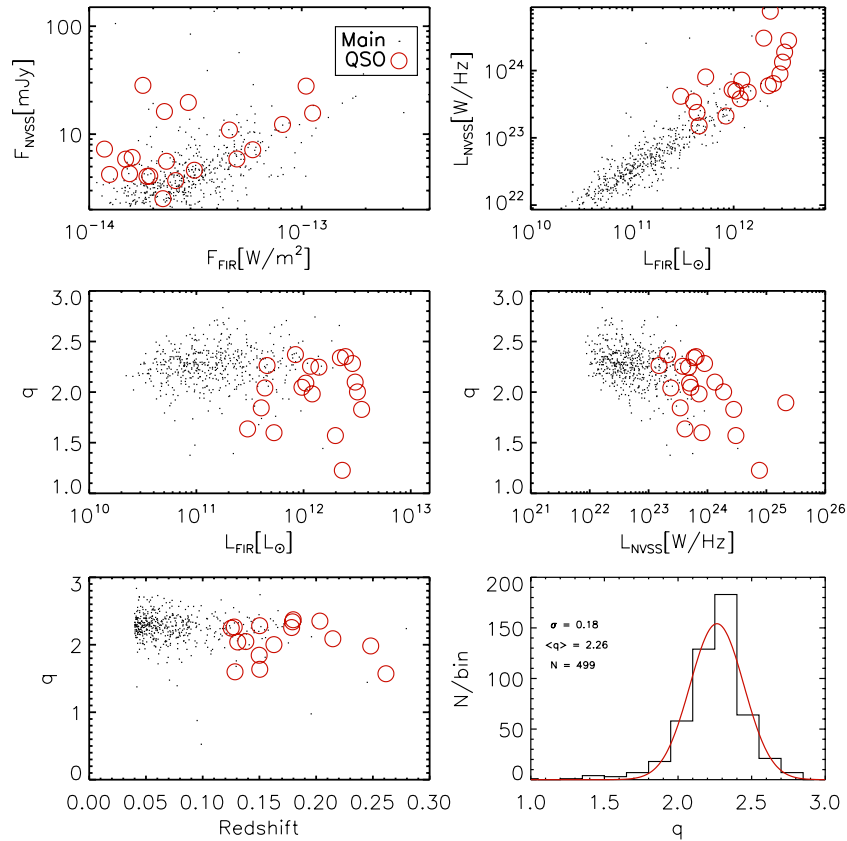
Figure 7. Radio–FIR correlation shown for the NVSS–SDSS–*IRAS* galaxies (dots) and quasars (open circles). The middle panels show the FIR/radio ratio (i.e., q parameter defined by Equation (1)) as a function of FIR (left) and radio (right) luminosities. Note a decrease in the q-value with increasing radio luminosity. The bottom panels show q as a function of redshift (left) and the distribution of q with its best-fit Gaussian (right). The number of objects in the sample (N), the biweighted mean FIR/radio ratio ($\langle q \rangle$), and the dispersion (σ) are indicated in the bottom right panel.

(A color version of this figure is available in the online journal.)

dominated by recent star formation. To shed light on the source of radio/FIR emission in our galaxies, in this section we investigate the correlation between their radio/FIR luminosities and SFRs, independently determined based on fitting stellar population synthesis models to the NUV-NIR SED).

We have derived an SFR for every galaxy in our sample by fitting the Bruzual et al. (2003) library of stellar population synthesis models to the SDSS *ugriz* photometry (see Section 2). In Figure 11, we show the radio and FIR luminosities of our sources as a function of our SED-based SFRs. As expected, a correlation is discernible between these two quantities. This is especially emphasized for star formation dominated galaxies (i.e., star-forming and composite galaxies), the distribution of which agrees well with the commonly used radio/IR luminosity—SFR calibrations (Kennicutt 1998; Yun et al. 2001). Note that this is quite remarkable as the SFRs have been derived completely independently from the FIR or radio emissions in the galaxies.

From Figure 11 it is obvious that a large fraction of galaxies with significant AGN contribution (Seyfert, LINER and absorption galaxies) has an obvious excess of radio power and FIR luminosity compared to that expected from the galaxy's SFR. The most obvious examples of this are the LINER and absorption galaxies from both the NVSS–SDSS and NVSS–SDSS–*IRAS* samples.

To investigate whether star formation is the underlying source of radio/FIR emission in our galaxies, we further quantify the difference between the radio/FIR emission and that expected

from star formation. We thus define an "excess" in radio/FIR emission relative to that expected from star formation ($\Delta \log L_{1.4 \, \text{GHz}}$ and $\Delta \log L_{\text{FIR}}$, resp.) as

$$\Delta \log L = \log L_{\text{data}} - \log L_{\text{exp}}, \qquad (5)$$

where $\log L_{\text{data}}$ is the logarithm of the 1.4 GHz or FIR luminosity derived based on NVSS or *IRAS* data (see Section 2), and $\log L_{\text{exp}}$ is the luminosity (either at 1.4 GHz or FIR) expected based on the SED-derived SFR and the standard radio and FIR luminosity to SFR calibrations. To convert SFR to radio luminosity we use the calibration defined in Yun et al. (2001): SFR $[M_\odot \, \text{yr}^{-1}] = 5.9 \times 10^{-22} \, L_{1.4 \, \text{GHz}}$ [W Hz^{-1}]. To convert SFR to FIR luminosity we use the standard conversion defined by Kennicutt (1998): SFR $[M_\odot \, \text{yr}^{-1}] = 4.5 \times 10^{-37} \, L_{\text{FIR}}$ [W]. Prior to applying these conversions, derived using a Salpeter IMF, we have scaled our SED-based SFRs by -0.2 dex to convert from a Chabrier to a Salpeter IMF (we have additionally included a scaling factor of ~ 0.4 dex to account for the star formation histories used in our models; see Smolčić et al. 2008 and Walcher et al. 2008 for details).

Figure 12 shows the FIR ($\Delta \log L_{\text{FIR}}$) versus 1.4 GHz ($\Delta \log L_{1.4 \, \text{GHz}}$) luminosity excess for different types of galaxies in the NVSS–SDSS–*IRAS* sample. As expected, star-forming galaxies follow a normal distribution in both the FIR and radio luminosity excess, with a mean $\Delta \log L$ value of about zero ($\langle \Delta \log L_{\text{FIR}} \rangle = 0.001$, $\langle \Delta \log L_{1.4 \, \text{GHz}} \rangle = 0.06$). The rms scatter is 0.35, and 0.32 for the FIR and radio distributions, respectively.
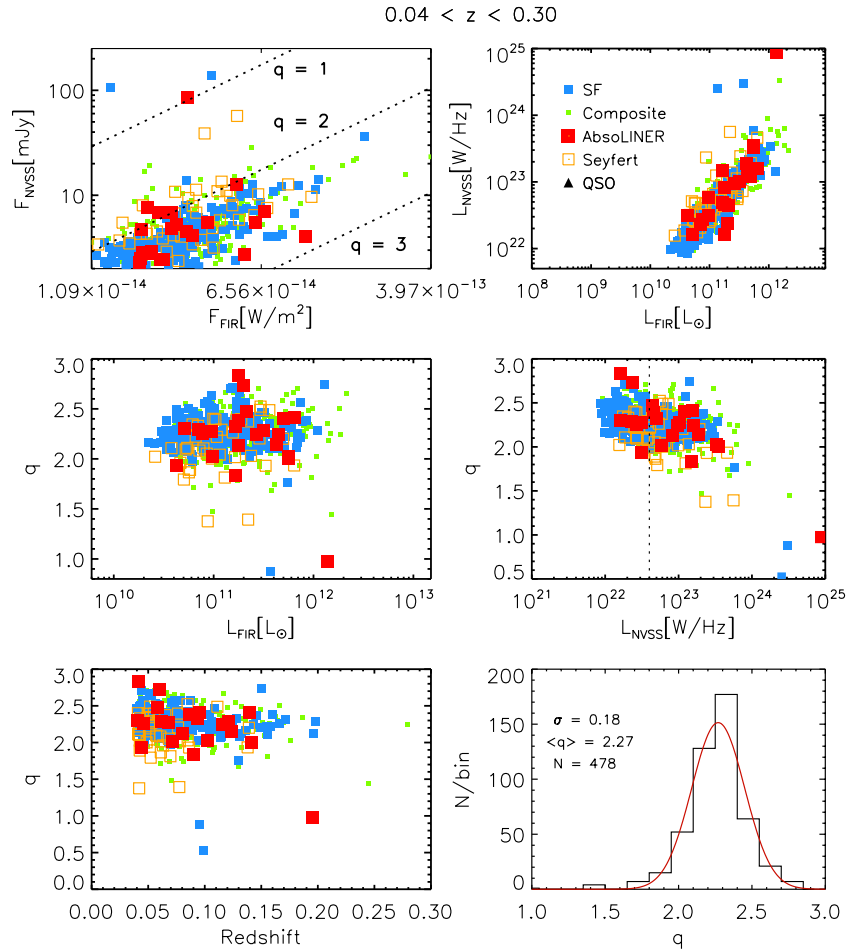
$$0.04 < z < 0.30$$

Figure 8. Equivalent to Figure 7, but for different galaxy types. The different symbols are indicated in the top right panel, and lines of constant q have been added to the top left panel.

(A color version of this figure is available in the online journal.)

Assuming the validity of the SFR to radio/FIR calibrations, such a (normal) distribution is expected if FIR and radio emissions arise from star formation processes in the galaxies. From Figure 12 it is apparent that, as the AGN contribution (defined via optical spectroscopic emission-line properties) rises in galaxies, the distribution of both the FIR and radio luminosity excess becomes highly skewed towards higher $\Delta \log L$ values. Although for a fraction of optically selected AGNs it is possible that the AGN contribution to the radio/FIR may be weak ($\Delta \log L \sim 0$), and they may be overwhelmed by star formation (which results in the canonical FIR/radio ratio), the significant skewness of the $\Delta \log L$ distributions suggests an additional source of radio and FIR emission in AGN-bearing galaxies (at least for $\Delta \log L > 0$). Even more interesting is that galaxies with large luminosity excess in both FIR and radio emission ($\Delta \log L \gtrsim 0.9$) predominantly have FIR/radio ratios consistent with the mean q-value for star-forming galaxies (see Figure 12). This will be discussed in more detail in Section 5.

5. DISCUSSION

5.1. Comparison with Previous Results

Extensive studies of the radio–FIR correlation (e.g., Helou et al. 1985; Condon 1992; Yun et al. 2001; Condon et al. 2002; Obrić et al. 2006; Mauch & Sadler 2007) have led to an average FIR/radio ratio in the local ($z < 0.3$) universe of $q \sim 2.3$, and

lower for AGN-bearing galaxies (see Table 2 in Sargent et al. 2010 for a summary). For example, using the *IRAS* 2 Jy galaxy sample ($F_{60\,\mu m} \geqslant 2$ Jy; 1809 sources with optical counterparts and well determined redshifts) combined with NVSS data, Yun et al. (2001) have found $\langle q \rangle = 2.34 \pm 0.01$. A lower average q-value is generally inferred when using radio-selected samples, and reaching fainter in the IR (see Sargent et al. 2010 for a detailed discussion of selection effects). Combining NVSS data with the optical Uppsala Galaxy Catalog (UGC) and the *IRAS* FSC and PSC, Condon et al. (2002) have found $\langle q \rangle = 2.3$ and rms width $\sigma = 0.18$. Furthermore, matching NVSS and 6dFGS survey data only with the *IRAS* FSC, Mauch & Sadler (2007) inferred a mean q-value of 2.28 with a rms scatter of 0.22 for their entire sample. For a subset of the radio-loud AGN (that would correspond to our Seyfert, LINER, absorption, and quasar classes combined), they found an even lower average value, $\langle q \rangle = 2.0$, and a significantly higher scatter in the FIR/radio ratio ($\sigma = 0.5$).

In Figure 9, we have presented the distribution of q for various types of our spectroscopically selected NVSS–SDSS-*IRAS* (PSC+FSC) galaxies. Our results yield that the dispersion is the tightest for star-forming galaxies ($\sigma = 0.13$), and rises by a factor of 1.5, 2.5, and 2.2 for composite, Seyfert, and absorption/LINER galaxies, respectively. We find that the average FIR/radio ratio for all objects in our radio–optical-IR sample is 2.27 ± 0.01 with a dispersion of 0.2. This is in very
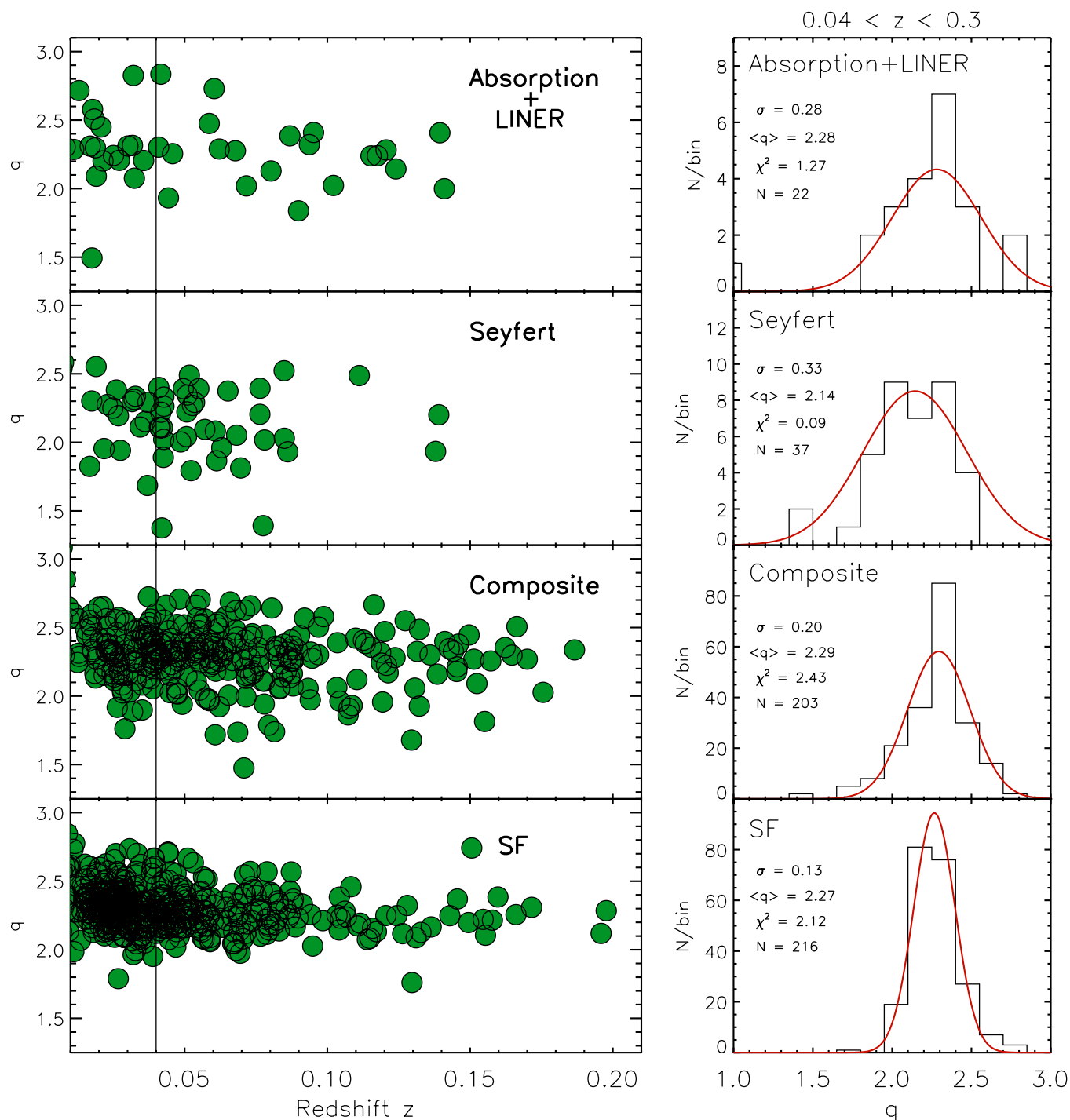
Figure 9. Radio–FIR correlation shown for the NVSS–SDSS–*IRAS* galaxies divided (from top to bottom) into (a) absorption line galaxies, (b) LINERs, (c) Seyferts, (d) composite, and (e) star-forming galaxies. The left panels show the FIR–radio correlation slope, q, as a function of redshift. The right panels show the distribution of q for each class of galaxies in the redshift range $0.04 < z < 0.3$, free of selection effects due to SDSS fiber sizes used for their optical spectroscopy.

(A color version of this figure is available in the online journal.)

good agreement with the results from Mauch & Sadler (2007). Furthermore, if we limit the 60 μm fluxes of our full sample to $\geqslant$2 Jy we obtain an average value of 2.34, consistent with that inferred by Yun et al. (2001).

Our results yield a lower FIR/radio ratio ($\langle q \rangle = 2.14 \pm 0.05$) for Seyfert galaxies, and a significantly higher rms scatter ($\sigma = 0.3$), compared to that found for SF galaxies. It is interesting that the mean q-value for our IR-detected LINER

and absorption line galaxies is comparable to that for star-forming galaxies. However, the spread in q for the former is significantly larger than for the latter (0.28 compared to 0.13, respectively). The average FIR/radio ratio for the 21 quasars in our sample is $q = 2.04$, comparable to that inferred for Seyferts and lower than that for star-forming galaxies. If we combine our AGN-bearing galaxies (quasars, Seyferts, LINERs, absorption galaxies) into one class in order to match the AGN
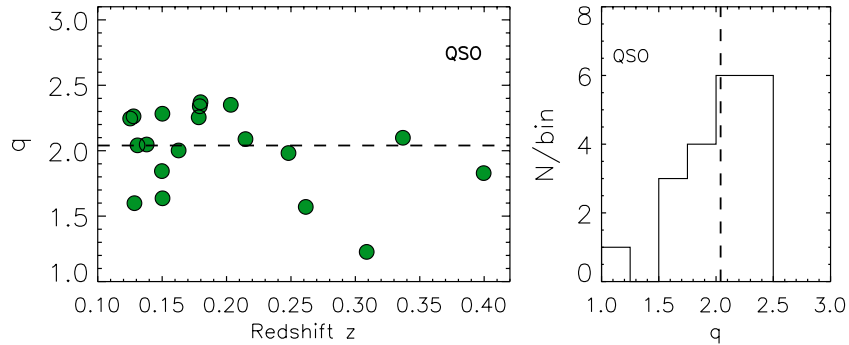
Figure 10. FIR/radio ratio (q) as a function of redshift (left panel) and the distribution of q for 21 IR (*IRAS*) detected quasars (right panel) in our radio–IR–optical sample. Note that the median q-value for quasars is lower than the average q obtained for star-forming galaxies, but comparable to that obtained for Seyfert galaxies (see Figure 9). The source with $q \sim -1$ is a strong radio source.
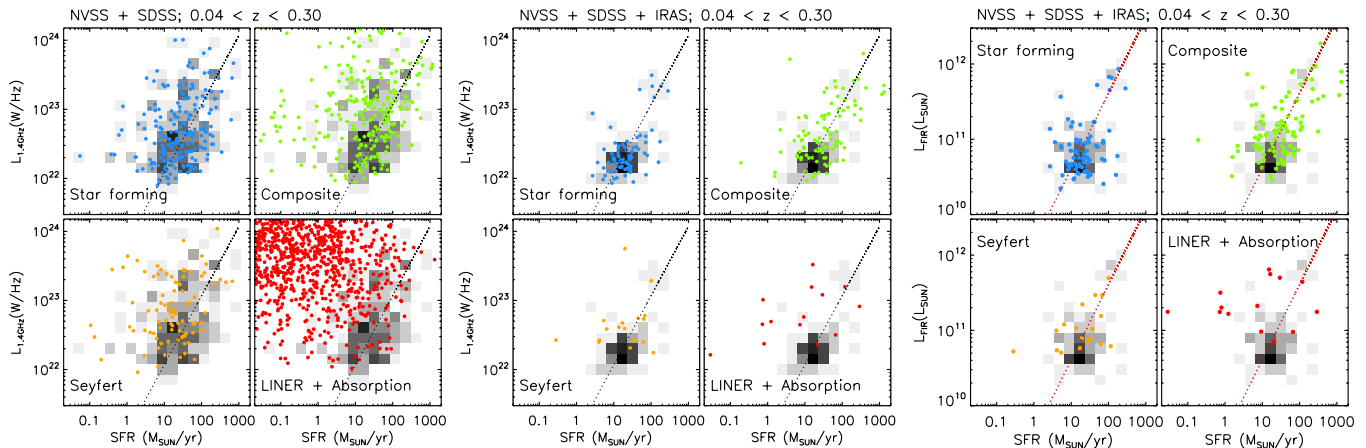
(A color version of this figure is available in the online journal.)

Figure 11. 1.4 GHz radio (left and middle panel) and FIR (right panel) luminosity as a function of SFR, derived via SED fitting to the NUV-NIR SDSS photometry (see the text for details). In the three large panels different galaxy types (symbols) and samples (indicated above and in each panel) are shown. The gray-scale histogram in each plot shows the distribution of star-forming galaxies for a given sample. Superimposed on the plots (dashed lines) are calibrations converting radio and FIR luminosity to SFR (Yun et al. 2001; Kennicutt 1998).

(A color version of this figure is available in the online journal.)

sample of Mauch & Sadler (2007), we infer an average q of 2.16 ± 0.03 (with an rms scatter of $\sigma = 0.24$). This is in relatively good agreement with their results. In the next sections we will discuss the variation of q with radio luminosity and the AGN contribution to the radio–FIR correlation.

5.2. AGN Contribution to the Radio–FIR Correlation

A low q-value is often used to discriminate between star-forming galaxies and AGNs. For example, Condon et al. (2002) have classified radio-loud AGNs as those having $q \leqslant 1.8$. Assuming that the FIR emission arises solely from star formation, this criterion selects galaxies with more than three times the radio emission from galaxies on the FIR–radio correlation. Yun et al. (2001) have used $q = 1.64$ as a star formation/AGN separator, identifying galaxies that emit in radio more than five times that predicted by the correlation. It is important to point out that these discriminating values are tuned to select only the most radio-loud AGN. Having (1) separated our NVSS–SDSS–*IRAS* sample into various classes of AGNs, and (2) independently estimated SFRs in their host galaxies, we can now analyze the physical source of FIR and radio emission in galaxies both following and offset from the radio–FIR correlation.

Assuming that the additional source of FIR and radio emission (relative to that expected from star formation) observed in our composite, Seyfert, absorption, and LINER galaxies (see Figure 12) arises from the central supermassive black hole, the distribution of our luminosity excess, $\Delta \log L$ defined in Equation (5), allows us to constrain the *average* contribution of star formation and AGN activity to the total power output for a given galaxy population. Taking that star formation and AGN activity are the two dominant FIR/radio emission generators, i.e., $L_{tot} = L_{SF} + L_{AGN}$, the average fractional contributions of these two sources ($\langle f_{SF} \rangle$ and $\langle f_{AGN} \rangle$) to the total power output can then be computed as $\langle f_{SF} \rangle = 10^{-\langle \Delta \log L \rangle}$ and $\langle f_{AGN} \rangle = 1 - \langle f_{SF} \rangle$, where $\langle \Delta \log L \rangle$ denotes the average (median) of the $\Delta \log L$ distribution (see Figure 12).

The median $\Delta \log L$ values and the fractional star formation/AGN contributions are summarized in Table 2. As expected, for star-forming galaxies we infer that the average contribution to FIR and radio emission due to star formation is 100%. We find that composite objects are dominated by star formation at the ~80%–90% level. Further, the FIR emission from Seyfert galaxies arises predominantly from star formation (~75%), while the AGN contribution to radio luminosity in Seyfert galaxies is about a factor of 2 higher in the radio than in the FIR (see Table 2). The latter explains the lower average q-value
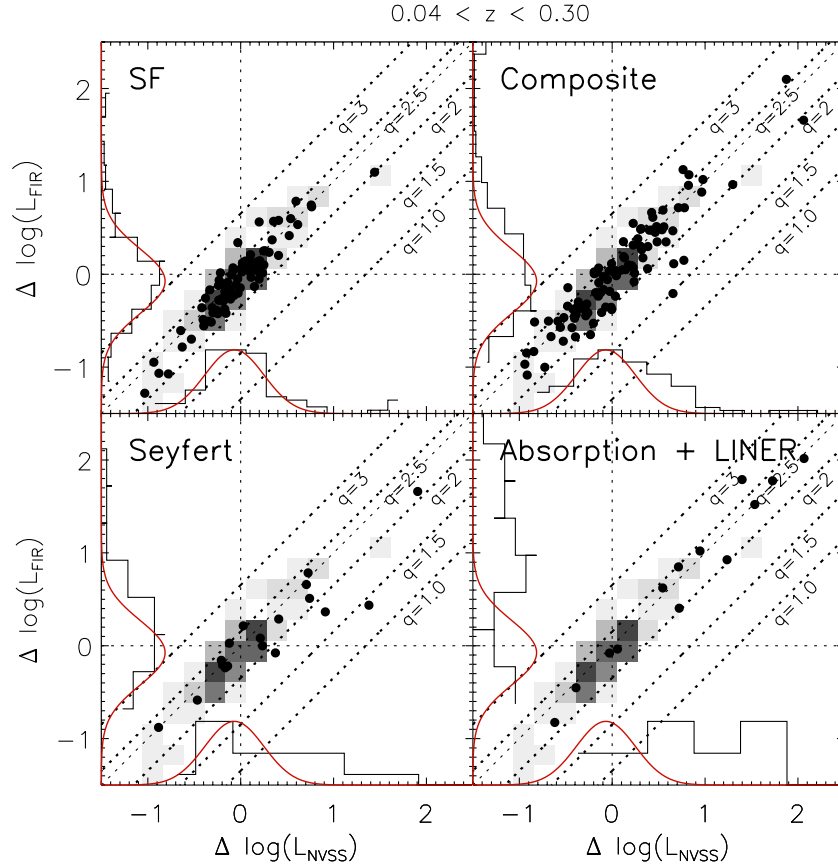
Figure 12. FIR excess ($\Delta \log L_{FIR}$) vs. radio excess ($\Delta \log L_{1.4\,GHz}$) for different types of NVSS–SDSS–*IRAS* galaxies (labeled in each panel) within a redshift range of 0.04–0.3. The FIR and radio excess has been defined as the difference in logarithm of the observed emission and that expected from their SFR, as given by the SED modeling (see Equation (5) and Figure 11 for details). Histograms on the axes show the distributions of the intrinsic $\Delta \log L$ values. A Gaussian fit to the distribution of *star-forming* galaxies is also shown in each panel (solid line). In each panel, filled dots represent the galaxies, and the gray scale shows the distribution of star-forming galaxies to guide the eye. Lines of constant q are also shown.

(A color version of this figure is available in the online journal.)

Table 2
Fractions of Star Formation and AGN Activity in Radio and FIR Regimes for
Various Types of Galaxies

Galaxy Types	Radio		FIR	
	SF	AGN	SF	AGN
SF	100%	0%	100%	0%
Composite	81.3%	18.7%	90.7%	9.3%
Seyfert	56.8%	43.2%	76.1%	23.9%
Abso+LINER	11.3%	88.7%	12.8%	87.2%

Notes. Fractional star formation/AGN contribution to the radio and FIR for different optically selected galaxy types. For each population the fractions were estimated in a statistical manner based on the distribution of the difference between a galaxy's SED-derived SFR and radio/FIR luminosity (see Figure 12 and the text for details).

(compared to the nominal value) for Seyfert galaxies inferred here, as well as in, e.g., Obrić et al. (2006) and Mauch & Sadler (2007). Lastly, based on the above calculation, IR-detected absorption and LINER galaxies are on average strongly dominated by AGN activity (∼90%) in both their FIR and radio emission although their average FIR/radio ratio is consistent with that expected for star-forming galaxies (see Figure 12).

One of the main results of this work is that, for the large majority of galaxies with radio and/or IR emission excess,

we infer q-values consistent with the average FIR/radio ratio found for star-forming galaxies (see Figure 12). Thus, although a significant AGN contribution is likely present in these galaxies (adding to both the FIR and radio emission), they would not be identified with a simple low-q discriminator value, as is commonly used to select a radio-loud AGN. Our results indicate that the FIR/radio ratio is not particularly sensitive to AGN contribution and that the radio–FIR correlation is a poor discriminant of AGN activity, except for the most powerful AGN. This is consistent with observations of several AGN-bearing galaxies in the high-redshift universe.

Based on an SED analysis, Riechers et al. (2009) find that both the radio and FIR luminosity in the $z = 3.9$ quasar APM08279+5255 are dominated by the central AGN, but that it has a q-value consistent with the local radio–FIR correlation. Furthermore, Murphy et al. (2009) have analyzed *Spitzer*-IRS spectra of a sample of 22 $0.6 \lesssim z \lesssim 2.6$ galaxies, composed of submillimeter galaxies, as well as X-ray and optically selected AGNs in GOODS-N. Making use of their Infrared Spectrograph (IRS) spectra, they have performed a thorough starburst-AGN decomposition for each object which allowed them to estimate the fractional AGN contribution to the total IR luminosity output of each source. They demonstrate that the four galaxies having the largest mid-IR AGN fractions (>60%) in their sample have q-values consistent with the canonical value. Furthermore, they find that the FIR/radio ratio shows no trend with the fractional

contribution of AGN activity in the galaxies in the IR, consistent with our results.

6. SUMMARY AND CONCLUSIONS

Based on a new radio–optical–IR catalog we have separated our radio- (NVSS) and IR- (*IRAS*) detected SDSS galaxies ($0.04 < z \lesssim 0.2$) into star-forming, composite, Seyfert, LINER, absorption line galaxies, and quasars, and we have performed an in-depth analysis of the radio–FIR correlation for various types of star-forming and AGN-bearing galaxies. Utilizing our NUV-NIR SED based SFRs in combination with FIR and radio luminosity (expected to directly trace star formation), we have statistically quantified the source of radio and FIR emission in the galaxies in our sample. We find that Seyfert galaxies and quasars have FIR/radio ratios lower than the canonical value for star-forming galaxies. This is due to an additional contribution to their radio continuum emission, which likely arises from their AGNs. We further show that FIR-detected absorption and LINER galaxies are on average strongly dominated by AGN activity in both their FIR and radio emission; however their average FIR/radio ratio is consistent with that expected for star-forming galaxies. In summary, our results imply that most AGN-containing galaxies in our sample have FIR/radio flux ratios indistinguishable from those of the star-forming galaxies. Thus, attempts to separate AGNs from star-forming galaxies by their FIR/radio flux ratios alone is a poor discriminant of AGN activity, except for the most powerful radio-loud AGN.

REFERENCES

Appleton, P. N. 2004, ApJS, 154, 147
Baldwin, J. A., Phillips, M. M., & Terlevich, R. 1981, PASP, 93, 5
Becker, R. H. 1995, ApJ, 450, 559
Bell, E. F. 2003, ApJ, 586, 794
Best, P. N., Kauffmann, G., Heckman, T. M., & Ivezić, Ž. 2005, MNRAS, 362, 9
Bruzual, G., & Charlot, S. 2003, MNRAS, 344, 1000
Chapman, S. C., Blain, A. W., Smail, I., & Ivison, R. J. 2005, ApJ, 622, 772
Condon, J. J. 1984, ApJ, 287, 461
Condon, J. J. 1992, ARA&A, 30, 575
Condon, J. J., Cotton, W. D., & Broderick, J. J. 2002, ApJ, 124, 675
Condon, J. J., Cotton, W. D., Greisen, E. W., Yin, Q. F., Perley, R. A., Taylor, G. B., & Broderick, J. J. 1998, AJ, 115, 1693
Garrett, M. A. 2002, A&A, 384, L19
Helou, G., Soifer, B. T., & Rowan-Robinson, M. 1985, ApJ, 298, L7
Ibar, E., et al. 2008, MNRAS, 386, 953
Ivison, R. J., et al. 2010, MNRAS, 402, 245
Kartaltepe, J. S., et al. 2010, ApJ, 709, 572
Kauffmann, G., et al. 2003, MNRAS, 346, 1055
Kennicutt, R. 1998, ARA&A, 36, 189
Kewley, L. J., Dopita, M. A., Sutherland, R. S., Heisler, C. A., & Trevena, J. 2001, ApJ, 556, 121
Kewley, L. J., Groves, B., Kauffmann, G., & Heckman, T. 2006, MNRAS, 372, 961
Kewley, L. J., Jansen, R. A., & Geller, M. J. 2005, PASP, 117, 227
Kimball, A. E., & Ivezić, Ž. 2008, AJ, 136, 684
Kovacs, S. C., et al. 2006, ApJ, 650, 592
Mauch, T., & Sadler, E. M. 2007, MNRAS, 375, 931
Michałowski, M. J., Watson, D., & Hjorth, J. 2010, ApJ, 712, 942
Moshir, et al. 1992, Explanatory Supplement to the IRAS Faint Source Survey, Version 2 (JPL D-10015; Pasadena, CA: Jet Propulsion Laboratory) (FSC)
Murphy, E. J. 2009, ApJ, 706, 482
Neugebauer, G., et al. 1984, ApJ, 278, L1
Obrić, M., et al. 2006, MNRAS, 370, 1677
Riechers, D. A., Walter, F., Carilli, C. L., & Lewis, G. F. 2009, ApJ, 690, 463
Sajina, A., et al. 2008, ApJ, 683, 659
Sanders, D. B., & Mirabel, I. F. 1996, ARA&A, 34, 749
Sargent, M. T., et al. 2010, ApJS, 186, 341
Schneider, D. P. 2007, AJ, 134, 102
Smolčić, V. 2009, ApJ, 699, L43
Smolčić, V., et al. 2008, ApJS, 177, 14
Solomon, P. M., & Vanden Bout, P. A. 2005, ARA&A, 43, 677
Strauss, M. A., Davis, M., Yahil, A., & Huchra, J. P. 1990, ApJ, 361, 49
Vlahakis, C., Eales, S., & Dunne, L. 2008, MNRAS, 379, 1042
Walcher, C. J., et al. 2008, A&A, 491, 713
York, D. G., et al. 2000, AJ, 120, 1579
Yun, M. S., Reddy, N. A., & Condon, J. J. 2001, ApJ, 554, 803